

Hire-MLP: Vision MLP via Hierarchical Rearrangement

Jianyuan Guo^{1,3,*}, Yehui Tang^{1,2,*}, Kai Han¹, Xinghao Chen¹,
Han Wu³, Chao Xu², Chang Xu³, Yunhe Wang¹

¹Noah’s Ark Lab, Huawei Technologies.

²Peking University. ³University of Sydney.

{jianyuan.guo, kai.han, yunhe.wang}@huawei.com.

Abstract

This paper presents Hire-MLP, a simple yet competitive vision MLP architecture via hierarchical rearrangement. Previous vision MLPs like MLP-Mixer are not flexible for various image sizes and are inefficient to capture spatial information by flattening the tokens. Hire-MLP innovates the existing MLP-based models by proposing the idea of hierarchical rearrangement to aggregate the local and global spatial information while being versatile for downstream tasks. Specifically, the inner-region rearrangement is designed to capture local information inside a spatial region. Moreover, to enable information communication between different regions and capture global context, the cross-region rearrangement is proposed to circularly shift all tokens along spatial directions. The proposed Hire-MLP architecture is built with simple channel-mixing MLPs and rearrangement operations, thus enjoys high flexibility and inference speed. Experiments show that our Hire-MLP achieves state-of-the-art performance on the ImageNet-1K benchmark. In particular, Hire-MLP achieves an 83.4% top-1 accuracy on ImageNet, which surpasses previous Transformer-based and MLP-based models with better trade-off for accuracy and throughput.

1 Introduction

Attention mechanism based transformers have shown their superiority in the realm of natural language processing in these years. Several recent works such as ViT [6] and DeiT [29] proposed to transfer the transformers into visual recognition tasks [7], and achieved awesome results which are comparable with conventional CNNs. However, the heavy computational burdens

*Equal Contribution.

caused by the self-attention module in transformers withdraw the transformers from better trade-off between accuracy and latency. Recently, models composed of only multi-layer perceptrons (MLPs) have been a new trend in vision community [27, 28], these mlp-based models can achieve comparable results while discarding the heavy attention module. For example, MLP-Mixer [27] extracts per-location information through MLPs which are applied to every image patches, and captures long-range information through MLPs which are applied across patches.

Although MLP-Mixer can obtain the global receptive field, there are two intractable flaws that prevent the model from becoming a more general model for vision tasks: (i) The number of the patches (tokens) will change as the input size changes, which means it cannot be directly fine-tuned at other resolutions which are different from those used in pre-training phase, making MLP-Mixer infeasible to be transferred into downstream vision tasks such as detection and segmentation. (ii) MLP-Mixer rarely explores the local information, which is demonstrated as an useful inductive bias in both CNN and transformer-based architectures [9, 32]. The above challenges naturally motivate us to explore an efficient MLP-based architecture which encodes both local and global information and is compatible with flexible input resolutions at the same time.

In this paper, We propose the Hire-MLP architecture, which innovates the existing MLP-based models using hierarchical rearrangement operations. It is a competitive and simple alternative, which does not need either variants of fully connected layer [2] nor complicated shift operations [17, 33], and is based entirely on MLPs that are repeatedly applied only across feature channels.

Taking the first challenge into account, the sequence of tokens in MLP-Mixer are denoted as $X \in \mathbb{R}^{HW \times C}$, where HW and C are the number of patches and the channels, respectively. MLP-Mixer [27] first uses a token-mixing MLP which acts on columns of X to map $\mathbb{R}^{HW} \mapsto \mathbb{R}^{HW}$, and then uses a channel-mixing MLP which acts on rows of X to map $\mathbb{R}^C \mapsto \mathbb{R}^C$. The parameters of the token-mixing MLP are configured by the number of patches HW , which depends on the resolution of input images. To tackle this challenge, we construct our Hire-MLP merely by channel-mixing MLPs applied on the channel dimension. To address the second challenge, we build the Hire-MLP block based on hierarchical rearrangements and channel-mixing MLPs. The hierarchical rearrangement operation consist of the inner-region rearrangement and the cross-region rearrangement, in which both the local and global information can be easily captured in both height and width directions. We first split the input tokens into multiple regions along the height/width directions, and leverage the inner-region rearrangement operation to shuffle the adjacent tokens into a one-dimensional vector, followed by two fully connected layers to capture local information within these features. After that, this one-dimensional vector is restored back to the initial arrangement. For the communication between tokens from different regions, a cross-region rearrangement is implemented by shifting all the tokens along a specific direction. Such hierarchical rearrangement module enables our model to obtain both local and global information, and can easily handle the flexible input resolutions, improving the

performance of MLP-based architectures.

To be specific, our Hire-MLP has a hierarchical architecture similar to conventional CNNs [9] and recently proposed transformers [19] to generate pyramid feature representations for other downstream tasks. The overall architecture is shown in Figure 1. After the first projection layer, the resulting feature $X \in \mathbb{R}^{H \times W \times C}$ is then fed into a sequence of Hire-MLP blocks. Hire Module is a key component in Hire-MLP block, which consists of three independent branches. The first two branches consist of a cross-region rearrange layer, an inter-region rearrange layer, two channel-mixing fully connected layers, then an inner-region restore layer and a cross-region restore layer to capture local and global information along specific dimension, *i.e.*, the height and width dimension. The last branch is built upon a simple channel-mixing fully connected layer to capture channel information. Compared to existing MLP-based models that spatially shift features in different directions [17, 33] or leverage a new cycle fully connected operator [2], our Hire-MLP only needs the simple channel-mixing MLPs and rearrangement operations.

Experiments show that our Hire-MLP can largely improve the classification performance of existing MLP-like models. For example, the small-sized Hire-MLP (Hire-MLP-S) attains an 81.8% top-1 accuracy on ImageNet without any extra training data. Scaling up the model to larger sizes, *i.e.* 58M and 96M parameters, we can further obtain 83.1% and 83.4% accuracy, respectively. The proposed Hire-MLP achieves a better accuracy-latency trade-off than prior MLP-based as well as transformer-based architectures.

2 Related work

CNN-based models. LeCun *et al.* proposed the classical LeNet [16] in 1990s, which has contained most of the basic components of modern CNNs (*e.g.*, convolution and pooling). AlexNet [15] achieved far higher performance than other methods in the ILSVRC 2012 contest, and then much attention were paid on CNN-based methods. VGGNet [23] constructed a plain model by stacking only convolutional layers with kernel size of 3×3 . GoogLeNet [24] designed an inception module which contains multiple branches to fuse features from diverse receptive fields. For training extremely deep neural architectures, ResNet [9, 10] skipped multiple layers with an identity projection for alleviating gradient vanishing or exploding. With the skip connection, extremely deep CNNs can be well trained (*e.g.*, more than 1000 layers) to achieve high performance. Beside accuracy, efficiency is vital for the practical implementation of CNNs models, especially on resource-limited devices such as mobile phones and wearable devices. MobileNet [12] adopted depth-wise separable convolutions for aggregating spatial information, and then different channels communicate with each other through 1×1 convolutions. ShuffleNet [38] introduced the shuffle operation to complement the information loss caused by group convolutions, such shuffle operation can exchange the information across different groups. These well-designed CNN architectures have been widely used in var-

ious computer vision tasks such as image recognition [?], object detection [22] and video analysis [14].

Transformer-based models. The classical transformer model [30] was originally designed to tackle natural language processing (NLP) tasks such as machine translation and English constituency parsing. Recently, Dosovitskiy *et al.* [6] introduced it to computer vision community by splitting an image into multiple patches and took each patch as a token in NLP. Vision transformers lack some of the inductive biases inherent to CNNs (*e.g.*, translation equivariance and locality). Thus they can accommodate more training data and achieve higher performance compared to CNN models when the training datasets are large enough. Touvron *et al.* [29] explored how to train data-efficient vision transformers and proposed a distillation strategy as well. Extensive works [31, 19, 8, 34] were proposed to design the architecture of vision transformers. For example, PVT [31] designed a pyramid-like structure containing multiple stages, and the spatial sizes of feature maps are reduced stage-by-stage. The PVT model validated the efficiency of vision transformers on dense prediction tasks, such as object detection and semantic segmentation. TNT [8] embedded small transformer blocks in the original modules to capture the local information and enhance the representation ability. T2T-ViT [35] improved the tokenization process of input images, and proposed a layer-wise Tokens-to-Token (T2T) transformation module by recursively aggregating neighboring Tokens. Compared to the simple tokenization with a single layer, the information of images can be preserved more sufficiently in the generated tokens. Considering that the high computational cost of the self-attention module, Swin Transformer [19] calculated the attention between different tokens in shifted local windows, which reduce the computational cost from quadratic to linear complexity. However, the self-attention mechanism is still computational expensive and relatively slow on devices like GPUs.

MLP-based models. Considering the large computational cost of attention modules in transformers, simple and efficient models that consist of only multi-layer perceptrons (MLPs) are proposed [27, 28]. For example, MLP-Mixer [27] used token-mixing MLP and channel-mixing MLP to capture the relationship between tokens and channels, respectively. Concurrently, the performance of MLP-based models are further improved by designing new architectures. CycleMLP [2] introduced a cycle fully connected layer to capture the spatial information, which replaces token-mixing MLP in [27]. AS-MLP [17] shifted tokens along vertical and horizontal directions to get an axial receptive field. S^2 -MLP [33] also used the shift operation to achieve cross-patch communications. Different from them, our method captures the spatial information by a hierarchical rearrangement operation, *i.e.*, rearranging tokens in/cross local regions, which achieves a better trade-off between high performance and computational efficiency.

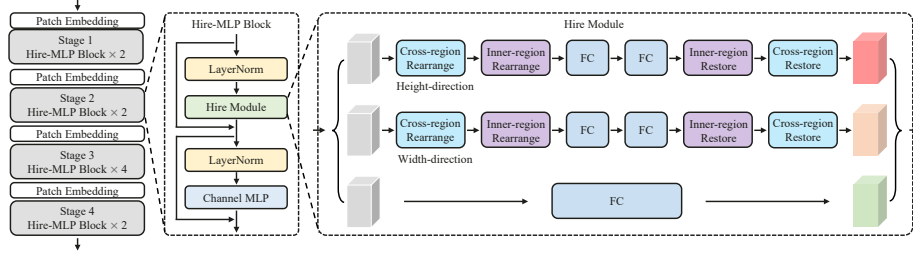


Figure 1: The overall architecture of the proposed Hire-MLP-Tiny. Table 1 shows more details and other variants.

3 Method

3.1 Hire-MLP Block

The proposed Hire-MLP architecture is constructed by stacking multiple Hire-MLP blocks, whose diagram illustration is shown in Figure 1. Similar to ViT [6] and MLP-Mixer [27], each Hire-MLP block composes of two sub-blocks, *i.e.*, the proposed Hire Module and Channel MLP in [27], which aggregates spatial information and channel information, respectively. Given the input feature $X \in \mathbb{R}^{H \times W \times C}$ with height H , width W and channel number C , a Hire-MLP block can be formulated as:

$$\begin{aligned} Y &= \text{Hire-Module}(\text{LN}(X)) + X, \\ Z &= \text{Channel-MLP}(\text{LN}(Y)) + Y, \end{aligned} \quad (1)$$

where Y, Z are intermediate feature and output feature of the block, respectively. LN denotes the layer normalization [1]. The whole Hire-MLP model is constructed by iteratively stacking the Hire-MLP block in Eq. 1. Compared with MLP-Mixer [27], the major difference is that token-mixing MLP in MLP-Mixer is replaced by the proposed Hire-Module to capture the relationship between different tokens effectively.

3.2 Hierarchical Rearrangement Module

In MLP-Mixer [27], the token-mixing MLP uses fully connected layers to capture cross-location information, which takes all the tokens as input. As the dimension of fully connected layers is fixed, it is not compatible with variable-length sequence of tokens on dense prediction tasks (*e.g.*, object detection and semantic segmentation). Besides, each token-mixing operation tries to capture the global information, while some crucial local information might be neglected. In this section, we propose a hierarchical rearrangement (dubbed as ‘Hire’) module to replace the token-mixing MLP in [27]. Each Hire Module focuses on tokens in a local region with an *inner-region rearrangement* operation while the global information can be *cross-region rearrangement*. The proposed Hire Module can tackle token sequence with variable lengths naturally.

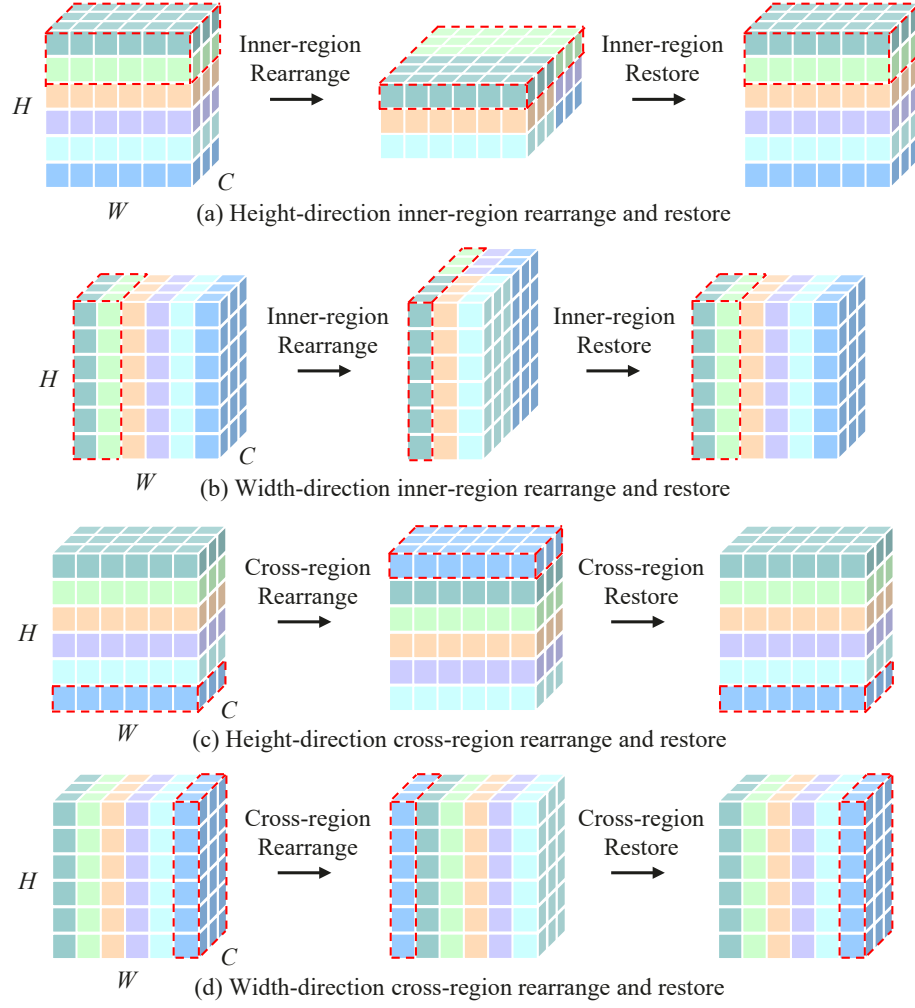


Figure 2: Illustration of the proposed rearrangement operations in Hire Module.

Table 1: **Variants of Hire-MLP architectures for ImageNet classification.** Hire-MLP blocks are shown in brackets, with the numbers of blocks stacked. H and W are the height and width of input image, respectively. s is the step size of token shift in cross-region rearrangement.

| | Size | Layer | Hire-MLP | | | |
|--------------|------------------------------------|-----------------|--|---|---|---|
| | | | Tiny | Small | Base | Large |
| Stage 1 | $\frac{H}{4} \times \frac{W}{4}$ | Patch Embedding | $[7 \times 7, 64]$ stride=4 | $[7 \times 7, 64]$ stride=4 | $[7 \times 7, 64]$ stride=4 | $[7 \times 7, 96]$ stride=4 |
| | | Hire-MLP Block | $\begin{bmatrix} h=4 \\ w=4 \\ s=2 \end{bmatrix} \times 2$ | $\begin{bmatrix} h=4 \\ w=4 \\ s=2 \end{bmatrix} \times 3$ | $\begin{bmatrix} h=4 \\ w=4 \\ s=2 \end{bmatrix} \times 4$ | $\begin{bmatrix} h=4 \\ w=4 \\ s=2 \end{bmatrix} \times 4$ |
| Stage 2 | $\frac{H}{8} \times \frac{W}{8}$ | Patch Embedding | $[3 \times 3, 128]$ stride=2 | $[3 \times 3, 128]$ stride=2 | $[3 \times 3, 128]$ stride=2 | $[3 \times 3, 192]$ stride=2 |
| | | Hire-MLP Block | $\begin{bmatrix} h=3 \\ w=3 \\ s=2 \end{bmatrix} \times 2$ | $\begin{bmatrix} h=3 \\ w=3 \\ s=2 \end{bmatrix} \times 4$ | $\begin{bmatrix} h=3 \\ w=3 \\ s=2 \end{bmatrix} \times 6$ | $\begin{bmatrix} h=3 \\ w=3 \\ s=2 \end{bmatrix} \times 6$ |
| Stage 3 | $\frac{H}{16} \times \frac{W}{16}$ | Patch Embedding | $[3 \times 3, 320]$ stride=2 | $[3 \times 3, 320]$ stride=2 | $[3 \times 3, 320]$ stride=2 | $[3 \times 3, 384]$ stride=2 |
| | | Hire-MLP Block | $\begin{bmatrix} h=3 \\ w=3 \\ s=1 \end{bmatrix} \times 4$ | $\begin{bmatrix} h=3 \\ w=3 \\ s=1 \end{bmatrix} \times 10$ | $\begin{bmatrix} h=3 \\ w=3 \\ s=1 \end{bmatrix} \times 24$ | $\begin{bmatrix} h=3 \\ w=3 \\ s=1 \end{bmatrix} \times 24$ |
| Stage 4 | $\frac{H}{32} \times \frac{W}{32}$ | Patch Embedding | $[3 \times 3, 512]$ stride=2 | $[3 \times 3, 512]$ stride=2 | $[3 \times 3, 512]$ stride=2 | $[3 \times 3, 768]$ stride=2 |
| | | Hire-MLP Block | $\begin{bmatrix} h=2 \\ w=2 \\ s=1 \end{bmatrix} \times 2$ | $\begin{bmatrix} h=2 \\ w=2 \\ s=1 \end{bmatrix} \times 3$ | $\begin{bmatrix} h=2 \\ w=2 \\ s=1 \end{bmatrix} \times 3$ | $\begin{bmatrix} h=2 \\ w=2 \\ s=1 \end{bmatrix} \times 3$ |
| # Parameters | | | 17.1M | 33.1M | 58.1M | 95.6M |
| # FLOPs | | | 2.1G | 4.2G | 8.1G | 13.5G |

Region Partition. We first split features into multiple regions, and the inner-region rearrangement is conducted on tokens in each region. The feature can be split along both width and height directions. Taking the height-dimension inner-region rearrangement as an example, the input feature X with shape $H \times W \times C$ can be divided into g regions, *i.e.*, $X = [X_1, X_2, \dots, X_g]$. Each region $X_i \in \mathbb{R}^{h \times W \times C}$ contains h tokens along the height direction, and $H = h \times g$.

Inner-Region Rearrangement. For feature X_i with shape $h \times W \times C$ in the i -th region along the height direction, the information of different tokens will communicate adequately with inner-region rearrangement operation. Specially, we concatenate different tokens in the region along the channel dimension, and get the rearranged feature X_i^c with shape $W \times hC$ (Figure 2(a)). Then the rearranged feature X_i^c is sent to a MLP module \mathcal{F} to mix information along the last dimension and get output feature $X_i^o \in \mathbb{R}^{W \times hC}$. For efficiency, the MLP \mathcal{F} is implemented by two linear projections with bottleneck, *i.e.*, the feature dimension is firstly reduced to $W \times \frac{C}{2}$ and then restored to $W \times hC$. A non-linear activation function (*e.g.*, ReLU, GeLU) and normalization layers (*e.g.*, BN, LN) can also be inserted into the linear projections to enhance representation ability and stabilize training. At last, the output feature $X_i^o \in \mathbb{R}^{W \times hC}$ is restored to the original shape, *i.e.*, it is split into multiple tokens along the last dimension to get feature $X_i' \in \mathbb{R}^{h \times W \times C}$. In each local region, different input tokens are mixed adequately to obtain out features.

Cross-Region Rearrangement. With inner-region rearrangement, the output tokens only involve input tokens in a local region, producing a local receptive field whose size depends on the size of each region. Here we design a cross-region rearrangement operation, which exchange information across different regions by shifting tokens.

The cross-region rearrangement along the height direction is shown in Figure 2(c). It is implemented by recurrently shifting all the tokens along a specific direction with a given step size s . After shifting, the tokens contained by a local region will change. To get a global receptive field, the cross-region rearrangement operations are inserted before the inner-region rearrangement operation every two blocks (Figure 1). The positions of tokens are also restored after ‘inner-region restoration’ to preserve the relative position between different tokens, as illustrated in Figure 2(c) and Figure 2(d).

Note that Zhang *et al.* [?] uses channel shuffle operation to communicate across different groups, which disorganizes channels totally. While our proposed cross-region rearrangement preserves the relative position between different tokens. We argue that the relative position is vital to achieve high representation ability. Different strategies for the cross-region communication are investigated in Section 4.2.

Hire Module. Considering that the input feature contains both height and width dimensions, the information communication along the width and height directions are conducted within two branches, respectively. Inspired by the shortcut in ResNet [9] and ViP [11], an extra branch without spatial communication is also added, where only a fully connected layer is implied along the

channel dimension. The input X is sent to the three branches to get features X'_W, X'_H, X'_C , respectively, and then the output feature X' is obtained by summing up these feature, *i.e.*, $X' = X'_W + X'_H + X'_C$, as depicted in Figure 1.

Complexity analysis. In each Hire Module, the fully connected layer (FC) consumes the major memory and computational cost. Given the input feature $X \in \mathbb{R}^{H \times W \times C}$ and consider the height-direction branch, we first split it into H/h regions with shape $h \times W \times C$, and set the channel dimension of bottleneck to $C/2$, thus this branch occupies $h \times C \times \frac{C}{2} \times 2 = hC^2$ parameters and $\frac{H}{h} \times W \times C \times \frac{C}{2} \times 2 = HWC^2$ FLOPs. Considering a Hire Module containing three branches (height, width, channel), the total parameters and FLOPs are $(2hC^2 + C^2)$ and $3HWC^2$, respectively.

3.3 Overall architecture

The overall architecture of the proposed Hire-MLP is presented in Table 1. Following that in CNNs [9, 23], vision transformer [31, 19], we also adopt a pyramid-like architecture. Specially, the whole architecture contains four stages, where the feature resolution reduces from $\frac{H}{4} \times \frac{W}{4}$ to $\frac{H}{32} \times \frac{W}{32}$ and the output dimension increases accordingly. The pyramid architecture aggregates the spatial feature for extracting semantic information, which can be applied to image classification, object detection, and semantic segmentation.

We develop diverse variants of Hire-MLP architectures with different memory and computational cost. The base model (Hire-MLP-Base) contains {4, 6, 24, 3} layers for each stage. The ‘Tiny’ and ‘Small’ variants have fewer layers to realize efficient implementation, while the ‘large’ variants have larger representation capacity to achieve high performance. Detailed configurations can also be found in Table 1.

4 Experiments

In this section, we investigate the effectiveness of Hire-MLP architectures by conducting experiments on classification task. We first compare the proposed Hire-MLP with previous state-of-the-art mlp-based models, and then we ablate the important design elements of Hire-MLP.

4.1 ImageNet Classification

Experimental Settings. we conduct experiments on the challenging ImageNet-1K [5] benchmark, which is a image classification benchmark containing 1.28M training images and 50K validation images of 1000 classes. Such a dataset is also utilized to conduct the ablation studies. For fair comparisons with recent works, we adopt the same training and augmentation strategy as that in DeiT [29], *i.e.* models are trained for 300 epochs using the AdamW [20] optimizer with weight decay 0.05 and the batch size of 1024. We use a linear

warmup for early 20 epochs, the initial learning rate is set to $1e-3$ and gradually drops to $1e-5$. The data augmentation methods include Rand-Augment [4], MixUp [37], CutMix [36], label smoothing [25], Random Erasing [39] and Drop-Path [13]. All models are trained on 8 NVIDIA Tesla V100 GPUs, we report the experimental results with single-crop Top-1 and Top-5 accuracy.

Main Results. We compare our proposed Hire-MLP with previous CNN-based, Transformer-based, and MLP-based models on Imagenet as shown in Table 2. The resolution of input image is set to 224×224 . For example, our Hire-MLP-Small achieves 81.8% top-1 accuracy with 4.2G Flops, which is better than all other existing MLP-based models. When compared to recently proposed AS-MLP [17] and CycleMLP [2], our Hire-MLP can obtain slightly better performances without any complicated shift operations or variants of fully connected layer. Scaling up our model to 8.1G and 13.5G can achieve 83.1% and 83.4% top-1 accuracy, respectively, indicating the benefit of Hire-MLP Block for capturing both local and global information. We also show the comparison with conventional CNN-based and transformer-based models. When compared to transformer-based models such as DeiT [29], Swin Transformer [19], and PVT [8], our model can get better results with a faster inference speed. When compared to CNN-based architectures such as RegNetY [21], our Hire-MLP can achieve better results with similar model size and computational cost. However, there is still a gap between our model and the state-of-the-art EfficientNet. We argue that MLP-based architecture has its unique advantages of simplicity and inference speed, and we believe MLP-based models also has a lot of room for improvement.

4.2 Ablation Studies

The core component in the Hire-MLP is the hierarchical rearrangement module. We conduct the ablation studies about the number of the regions in region partition, the number of the shifted regions in cross-region rearrangement, and the padding mode in inner-region rearrangement. All ablation experiments are conducted based on the Hire-MLP-Small, as shown in the Table 1.

The number of regions in region partition. Table 3 investigates how region partition affects the final performance, where h and w denote the size of each region. Consider that the resolution of input image is always 224×224 , we set $h = w$ if not specified. A small region size implies few adjacent tokens are mixed adequately via the inner-region operation, which emphasizes more about local information. We empirically find that larger region sizes are required in lower layers to tackle the feature maps with more tokens and obtain larger receptive fields. When further increase the region size, the performance will drop slightly, we conjecture that there might be some information loss in the bottleneck structure with the increasing region size.

The step size s of token shift in cross-region rearrangement. The cross-region rearrangement is implemented by shifting tokens with a given step size s , whose impact is investigated in Table 4. When the tokens are not shifted ($s = 0$), there is no communication between different regions, which incur the bad performance obviously.

The impacts of different padding methods. For classification on ImageNet, the resolution of the input image is of size 224×224 , thus the shape of the feature in stage 4 is 7×7 , which is not divisible by any h and w . Thus we need to pad such feature map. Here we evaluate the influence of different padding methods, the corresponding results are shown in Table 5. We find that "Circular padding" is more suitable for the design of our Hire Module.

The impacts of different components in Hire Module. Table 6 ablates the impacts of different components in Hire Module. We can find that the inner-region rearrange is the most important component to capture local information. If we discard the cross-region rearrangement, the model cannot exchange information across different regions and the performance will drop to 81.06%.

Different strategies for cross-region communication. We compare two different strategies for cross-region communication in Table 7. The shifted manner achieves better result compared to ShuffleNet manner, indicating that the shifted manner can preserve more relative position information for model.

5 Conclusion

This paper proposes a novel variant of MLP-like architecture via hierarchically rearranging tokens for aggregating spatial information. The input features are split into multiple regions along the height/width directions. The different tokens in each region communicate adequately via the inner-region rearrangement, which mixes channels from different tokens to extract local information. Tokens from different regions are rearranged by token shift, which exchanges the information between regions, but also preserves their relative positions. Based on the two rearrangement operations, a effective but efficient MLP-like model is constructed, which achieve obvious performance improvement on the existing methods.

Table 2: The experimental results of different networks on ImageNet-1K. Throughput is measured with the batch size of 64 on a single V100 GPU, following [29]. [†] means the throughput result is reproduced by us.

| Network | # Params | # FLOPs | Top-1 (%) | Top-5 (%) | Throughput (image / s) |
|-------------------------------|----------|---------|-------------|-----------|---------------------------|
| CNN-based | | | | | |
| RegNetY-4GF [21] | 39M | 4.0G | 81.0 | - | 1156.7 |
| RegNetY-16GF [21] | 84M | 16.0G | 82.9 | - | 334.7 |
| EfficientNet-B4 [26] | 19M | 4.2G | 82.9 | 96.4 | 349.4 |
| EfficientNet-B5 [26] | 30M | 9.9G | 83.6 | 96.7 | 169.1 |
| EfficientNet-B6 [26] | 43M | 19.0G | 84.0 | 96.8 | 96.9 |
| Transformer-based | | | | | |
| DeiT-S [29] | 22M | 4.6G | 79.8 | - | 940.4 |
| T2T-ViT _t -14 [34] | 22M | 5.2G | 80.7 | - | - |
| Swin-T [19] | 29M | 4.5G | 81.3 | - | 755.2 |
| CPVT-S-GAP [3] | 22M | 4.6G | 81.5 | - | 942.3 |
| TNT-S [8] | 24M | 5.2G | 81.5 | 95.7 | - |
| PVT-M [31] | 44M | 6.7G | 81.2 | - | 528.1 |
| PVT-L [31] | 61M | 9.8G | 81.7 | - | 358.8 |
| T2T-ViT _t -24 [34] | 65M | 15.0G | 82.6 | - | - |
| TNT-B [8] | 66M | 14.1G | 82.9 | 96.3 | - |
| Swin-B [19] | 88M | 15.4G | 83.5 | - | 278.1 |
| MLP-based | | | | | |
| gMLP-Ti [18] | 6M | 1.4G | 72.3 | - | - |
| CycleMLP-B1 [2] | 15M | 2.1G | 78.9 | - | 1212.0 [†] |
| Hire-MLP-Ti (ours) | 17M | 2.1G | 78.9 | 94.5 | 1661.2 |
| ResMLP-S12 [28] | 15M | 3.0G | 76.6 | - | 1415.1 |
| ViP-Small/7 [11] | 25M | - | 81.5 | - | 719.0 |
| AS-MLP-T [17] | 28M | 4.4G | 81.3 | - | 1047.7 |
| CycleMLP-B2 [2] | 27M | 3.9G | 81.6 | - | 776.8 [†] |
| Hire-MLP-S (ours) | 33M | 4.2G | 81.8 | 95.9 | 893.2 |
| Mixer-B/16 [27] | 59M | 12.7G | 76.4 | - | - |
| S ² -MLP-deep [33] | 51M | 10.5G | 80.7 | 95.4 | - |
| ResMLP-B24 [28] | 116M | 23.0G | 81.0 | - | 231.3 |
| ViP-Medium/7 [11] | 55M | - | 82.7 | - | 418.0 |
| AS-MLP-S [17] | 50M | 8.5G | 83.1 | - | 619.5 |
| Hire-MLP-B (ours) | 58M | 8.1G | 83.1 | 96.3 | 514.7 |
| S ² -MLP-wide [33] | 71M | 14.0G | 80.0 | 94.8 | - |
| CycleMLP-B5 [2] | 76M | 12.3G | 83.2 | - | 319.9 [†] |
| gMLP-B [18] | 73M | 15.8G | 81.6 | - | - |
| ViP-Large/7 [11] | 88M | - | 83.2 | - | 298.0 |
| AS-MLP-B [17] | 88M | 15.2G | 83.3 | - | 455.2 |
| Hire-MLP-L (ours) | 96M | 13.5G | 83.4 | 96.5 | 385.9 |

Table 3: Number of regions in region partition. Given an input feature of size $H \times W \times C$, we split it into H/h regions along with height-direction, each region is of size $h \times W \times C$. For example, (4, 3, 3, 2) indicates h and w are set to be 4, 3, 3, 2 for stage 1, stage 2, stage 3, and stage 4, respectively. We set $h = w$ as default for 224×224 input resolution. The step size s here is set to (1, 1, 1, 1).

| Number of h and w | Top-1 (%) |
|-----------------------|--------------|
| (2, 2, 2, 2) | 80.95 |
| (3, 2, 2, 2) | 81.04 |
| (3, 3, 2, 2) | 81.33 |
| (3, 3, 3, 2) | 81.58 |
| (3, 3, 3, 3) | 81.51 |
| (4, 3, 3, 2) | 81.69 |
| (4, 3, 3, 3) | 81.50 |
| (4, 4, 3, 3) | 81.35 |
| (5, 4, 3, 3) | 81.16 |

Table 4: Number of shifted regions in cross-region rearrangement. For example, (2, 2, 1, 1) indicates s is set to be 2, 2, 1, 1 for stage 1, stage 2, stage 3, and stage 4, respectively. And (0, 0, 0, 0) means there is no cross-region rearrangement in Hire-MLP. The h and w here is set to (4, 3, 3, 2).

| Number of shifted regions | Top-1 (%) |
|---------------------------|--------------|
| (0, 0, 0, 0) | 81.06 |
| (1, 1, 1, 1) | 81.53 |
| (2, 2, 1, 1) | 81.78 |
| (2, 2, 2, 2) | 81.46 |

Table 5: Different padding modes of inner-region rearrangement.

| Padding mode | Top-1 (%) |
|--------------------|--------------|
| Zero padding | 81.59 |
| Circular padding | 81.78 |
| Reflect padding | 81.36 |
| Replicated padding | 81.42 |

Table 6: Impact of different components in Hire Module.

| Model | Top-1 (%) |
|--------------------------------|--------------|
| Hire-MLP-Small | 81.78 |
| w/o cross-region rearrangement | 81.06 |
| w/o inner-region rearrangement | 79.81 |
| w/o channel-mixing | 81.18 |

Table 7: Impact of different methods for cross-region communication.

| Model | Top-1 (%) |
|-------------------|--------------|
| Shifted manner | 81.78 |
| ShuffleNet manner | 80.82 |

References

- [1] Jimmy Lei Ba, Jamie Ryan Kiros, and Geoffrey E Hinton. Layer normalization. *arXiv preprint arXiv:1607.06450*, 2016.
- [2] Shoufa Chen, Enze Xie, Chongjian Ge, Ding Liang, and Ping Luo. Cyclempl: A mlp-like architecture for dense prediction. *arXiv preprint arXiv:2107.10224*, 2021.
- [3] Xiangxiang Chu, Bo Zhang, Zhi Tian, Xiaolin Wei, and Huaxia Xia. Conditional positional encodings for vision transformers. *arXiv preprint arXiv:2102.10882*, 2021.
- [4] Ekin D Cubuk, Barret Zoph, Jonathon Shlens, and Quoc V Le. Randaugment: Practical automated data augmentation with a reduced search space. In *Proceedings of the IEEE/CVF Conference on Computer Vision and Pattern Recognition Workshops*, 2020.
- [5] Jia Deng, Wei Dong, Richard Socher, Li-Jia Li, Kai Li, and Li Fei-Fei. Imagenet: A large-scale hierarchical image database. In *2009 IEEE conference on computer vision and pattern recognition*, 2009.
- [6] Alexey Dosovitskiy, Lucas Beyer, Alexander Kolesnikov, Dirk Weissenborn, Xi-aohua Zhai, Thomas Unterthiner, Mostafa Dehghani, Matthias Minderer, Georg Heigold, Sylvain Gelly, et al. An image is worth 16x16 words: Transformers for image recognition at scale. *arXiv preprint arXiv:2010.11929*, 2020.
- [7] Kai Han, Yunhe Wang, Hanting Chen, Xinghao Chen, Jianyuan Guo, Zhenhua Liu, Yehui Tang, An Xiao, Chunjing Xu, Yixing Xu, et al. A survey on visual transformer. *arXiv preprint arXiv:2012.12556*, 2020.
- [8] Kai Han, An Xiao, Enhua Wu, Jianyuan Guo, Chunjing Xu, and Yunhe Wang. Transformer in transformer. *arXiv preprint arXiv:2103.00112*, 2021.
- [9] Kaiming He, Xiangyu Zhang, Shaoqing Ren, and Jian Sun. Deep residual learning for image recognition. In *Proceedings of the IEEE conference on computer vision and pattern recognition*, pages 770–778, 2016.
- [10] Kaiming He, Xiangyu Zhang, Shaoqing Ren, and Jian Sun. Identity mappings in deep residual networks. In *European conference on computer vision*, pages 630–645, 2016.
- [11] Qibin Hou, Zihang Jiang, Li Yuan, Ming-Ming Cheng, Shuicheng Yan, and Jiashi Feng. Vision permutator: A permutable mlp-like architecture for visual recognition. *arXiv preprint arXiv:2106.12368*, 2021.
- [12] Andrew G Howard, Menglong Zhu, Bo Chen, Dmitry Kalenichenko, Weijun Wang, Tobias Weyand, Marco Andreetto, and Hartwig Adam. Mobilenets: Efficient convolutional neural networks for mobile vision applications. *arXiv preprint arXiv:1704.04861*, 2017.
- [13] Gao Huang, Yu Sun, Zhuang Liu, Daniel Sedra, and Kilian Q Weinberger. Deep networks with stochastic depth. In *European conference on computer vision*, 2016.
- [14] Andrej Karpathy, George Toderici, Sanketh Shetty, Thomas Leung, Rahul Sukthankar, and Li Fei-Fei. Large-scale video classification with convolutional neural networks. In *Proceedings of the IEEE conference on Computer Vision and Pattern Recognition*, pages 1725–1732, 2014.
- [15] Alex Krizhevsky, Ilya Sutskever, and Geoffrey E Hinton. Imagenet classification with deep convolutional neural networks. *Advances in neural information processing systems*, pages 1097–1105, 2012.
- [16] Yann LeCun, Léon Bottou, Yoshua Bengio, and Patrick Haffner. Gradient-based learning applied to document recognition. *Proceedings of the IEEE*, 86(11):2278–2324, 1998.

- [17] Dongze Lian, Zehao Yu, Xing Sun, and Shenghua Gao. As-mlp: An axial shifted mlp architecture for vision. *arXiv preprint arXiv:2107.08391*, 2021.
- [18] Hanxiao Liu, Zihang Dai, David R So, and Quoc V Le. Pay attention to mlps. *arXiv preprint arXiv:2105.08050*, 2021.
- [19] Ze Liu, Yutong Lin, Yue Cao, Han Hu, Yixuan Wei, Zheng Zhang, Stephen Lin, and Baining Guo. Swin transformer: Hierarchical vision transformer using shifted windows. *arXiv preprint arXiv:2103.14030*, 2021.
- [20] Ilya Loshchilov and Frank Hutter. Decoupled weight decay regularization. *arXiv preprint arXiv:1711.05101*, 2017.
- [21] Ilija Radosavovic, Raj Prateek Kosaraju, Ross Girshick, Kaiming He, and Piotr Dollár. Designing network design spaces. In *Proceedings of the IEEE/CVF Conference on Computer Vision and Pattern Recognition*, 2020.
- [22] Shaoqing Ren, Kaiming He, Ross Girshick, and Jian Sun. Faster r-cnn: Towards real-time object detection with region proposal networks. *Advances in neural information processing systems*, 28:91–99, 2015.
- [23] Karen Simonyan and Andrew Zisserman. Very deep convolutional networks for large-scale image recognition. *arXiv preprint arXiv:1409.1556*, 2014.
- [24] Christian Szegedy, Wei Liu, Yangqing Jia, Pierre Sermanet, Scott Reed, Dragomir Anguelov, Dumitru Erhan, Vincent Vanhoucke, and Andrew Rabinovich. Going deeper with convolutions. In *Proceedings of the IEEE conference on computer vision and pattern recognition*, pages 1–9, 2015.
- [25] Christian Szegedy, Vincent Vanhoucke, Sergey Ioffe, Jon Shlens, and Zbigniew Wojna. Rethinking the inception architecture for computer vision. In *Proceedings of the IEEE conference on computer vision and pattern recognition*, 2016.
- [26] Mingxing Tan and Quoc Le. Efficientnet: Rethinking model scaling for convolutional neural networks. In *International Conference on Machine Learning*, 2019.
- [27] Ilya Tolstikhin, Neil Houlsby, Alexander Kolesnikov, Lucas Beyer, Xiaohua Zhai, Thomas Unterthiner, Jessica Yung, Daniel Keysers, Jakob Uszkoreit, Mario Luccic, et al. Mlp-mixer: An all-mlp architecture for vision. *arXiv preprint arXiv:2105.01601*, 2021.
- [28] Hugo Touvron, Piotr Bojanowski, Mathilde Caron, Matthieu Cord, Alaaeldin El-Nouby, Edouard Grave, Armand Joulin, Gabriel Synnaeve, Jakob Verbeek, and Herve Jegou. Resmlp: Feedforward networks for image classification with data-efficient training. *arXiv preprint arXiv:2105.03404*, 2021.
- [29] Hugo Touvron, Matthieu Cord, Matthijs Douze, Francisco Massa, Alexandre Sablayrolles, and Hervé Jégou. Training data-efficient image transformers & distillation through attention. *arXiv preprint arXiv:2012.12877*, 2020.
- [30] Ashish Vaswani, Noam Shazeer, Niki Parmar, Jakob Uszkoreit, Llion Jones, Aidan N Gomez, Lukasz Kaiser, and Illia Polosukhin. Attention is all you need. In *Advances in neural information processing systems*, pages 5998–6008, 2017.
- [31] Wenhai Wang, Enze Xie, Xiang Li, Deng-Ping Fan, Kaitao Song, Ding Liang, Tong Lu, Ping Luo, and Ling Shao. Pyramid vision transformer: A versatile backbone for dense prediction without convolutions. *arXiv preprint arXiv:2102.12122*, 2021.
- [32] Tete Xiao, Mannat Singh, Eric Mintun, Trevor Darrell, Piotr Dollár, and Ross Girshick. Early convolutions help transformers see better. *arXiv preprint arXiv:2106.14881*, 2021.
- [33] Tan Yu, Xu Li, Yunfeng Cai, Mingming Sun, and Ping Li. S2-mlp: Spatial-shift mlp architecture for vision. *arXiv preprint arXiv:2106.07477*, 2021.

- [34] Li Yuan, Yunpeng Chen, Tao Wang, Weihao Yu, Yujun Shi, Francis EH Tay, Jiashi Feng, and Shuicheng Yan. Tokens-to-token vit: Training vision transformers from scratch on imagenet. *arXiv preprint arXiv:2101.11986*, 2021.
- [35] Li Yuan, Yunpeng Chen, Tao Wang, Weihao Yu, Yujun Shi, Francis EH Tay, Jiashi Feng, and Shuicheng Yan. Tokens-to-token vit: Training vision transformers from scratch on imagenet. *arXiv preprint arXiv:2101.11986*, 2021.
- [36] Sangdoo Yun, Dongyoon Han, Seong Joon Oh, Sanghyuk Chun, Junsuk Choe, and Youngjoon Yoo. Cutmix: Regularization strategy to train strong classifiers with localizable features. In *Proceedings of the IEEE/CVF International Conference on Computer Vision*, 2019.
- [37] Hongyi Zhang, Moustapha Cisse, Yann N Dauphin, and David Lopez-Paz. mixup: Beyond empirical risk minimization. *arXiv preprint arXiv:1710.09412*, 2017.
- [38] Xiangyu Zhang, Xinyu Zhou, Mengxiao Lin, and Jian Sun. Shufflenet: An extremely efficient convolutional neural network for mobile devices. In *Proceedings of the IEEE conference on computer vision and pattern recognition*, pages 6848–6856, 2018.
- [39] Zhun Zhong, Liang Zheng, Guoliang Kang, Shaozi Li, and Yi Yang. Random erasing data augmentation. In *Proceedings of the AAAI Conference on Artificial Intelligence*, 2020.